Complexity in earthquake sequences controlled by multi-scale heterogeneity in fault fracture energy

Hideo Aochi, Satoshi Ide

Complexity in earthquake sequences controlled by multi-scale heterogeneity in fault fracture energy

Hideo Aochi

Land Planning and Natural Risks Division, BRGM, 3 avenue Claude Guillemin, Orléans 45060 Cedex, France. (h.aochi@brgm.fr)

Satoshi Ide

Earth and Planetary Science, The University of Tokyo, 7-3-1 Hongo, Bunkyo-ku, Tokyo 113-0033, Japan. (ide@eps.s.u-tokyo.ac.jp)

Abstract

A series of dynamic rupture events under constant tectonic loading is simulated on a fault with multi-scale heterogeneity and a stochastic rupture initiation process. The fracture energy of the fault plane is assumed to have multi-scale heterogeneous distribution using fractal circular patches. The stochastic rupture initiation process as a function of the accumulated stress is introduced in order to take account of unknown smaller-scale heterogeneity and variability. Five realizations of a statistical spatial distribution of fracture energy (fault heterogeneity maps) are tested for the simulations of earthquake sequences during a few seismic cycles. The diversity of earthquake sequences is principally controlled by the spatial distribution of the patches. The effect

of dynamic rupture appears in the residual stress after the characteristic events due to their directivity and this localizes the subsequent sequences. Although the characteristic earthquakes occur rather regularly in time and similarly in different seismic cycles, some irregular behavior is found, based on the heterogeneity maps and the randomness of the preceding earthquake sequence, leading to a visible anomaly in the seismicity. Such anomalies are not predicable, but understandable through the analysis of the considered earthquakes during the cycle. The similarity and the diversity simulated in this study, governed by the structure of an inherent distribution of multi-scale heterogeneity, suggests the importance of the pre-existing heterogeneity field along the fault for the appearance of earthquake sequences, including those that are characteristic.

1. Introduction

Most numerical studies of earthquake source dynamics have been based on a fixed observation scale, namely the assumption of characteristic, or fixed-scale, fault parameters for a target event; while there are few examples considering multi-scalability of fault parameters (e.g. Andrews, 1976; Aochi and Ide, 2004; Ide and Aochi, 2005; Andrews, 2005). Some spatial heterogeneity on a fault plane is often given in terms of stress and/or fault strength to explain the complexity of event (e.g. Mikumo and Miyatake, 1979; Olsen et al., 1997; Fukuyama and Madariaga, 1998; Guatteri et al., 2003; Oglesby and Day, 2005; Ripperger et al., 2007; and many others). The heterogeneous stress field has recently been also attributed to the complex fault geometry due to the irregular topography with respect to a tectonic force (e.g. Aochi and Fukuyama, 2002) and/or the history of past events (e.g. Duan and Oglesby, 2005; Shaw and Dieterich, 2007). As is natural, no detail smaller than an assumed model grid

size can be taken into account.

Recently, Ide and Aochi (2005) pointed out that multi-scale heterogeneity is essential in modeling wide-scale self-similarity of the earthquake source process (e.g., Ide and Beroza, 2001; Uchide and Ide, 2007), which cannot be modeled by a viewpoint at a single scale. Such multi-scale heterogeneity should be able to be introduced in the fracture energy of the fault surface, or simply in the critical slip distance D_c of a slip-weakening law considering that fault strength is approximately constant and independent of the scales. The fracture energy is estimated as from 1 J/m^2 in laboratory experiments (Atkinson, 1984; Ohnaka, 2003) to 1 MJ/m^2 for large earthquakes (Beroza and Spudich, 1988; Ide 2002). Linearly increasing G_c in a uniformly strained medium produces a self-similar rupture propagation and thus explains the scale-independency of rupture propagation velocity and slip velocity within the ruptured area (e.g. Andrews, 1976; Aochi and Ide, 2004). Such scaling in fracture energy can be explained by the fractal nature of fault surface roughness (Matsu'ura et al., 1992; Ohnaka, 2003; Ide and Aochi, 2005), while there are other possible interpretations such as purely mechanical effects between cracks (Yamashita and Fukuyama, 1996) or anelastic effects off the rupture plane (Andrews, 2005). Our model in this study is based on the former, namely that fracture energy is regarded as an intrinsic parameter given in advance. On a fault with a hierarchical G_c distribution, a rupture propagates self-similarly and stops without special mechanisms because the rupturing area is always covered by an area of larger D_c except for the largest characteristic earthquake of the system (Ide and Aochi, 2005). This does not mean that other heterogeneity in stress or other parameters in the friction law are not important; however, there are few studies focusing on the fracture energy and, therefore, it should be worth studying. The importance of this scaling problem is

shown by its influence on the radiated seismic waves from a fault (e.g. Mai et al., 2006). This paper considers how this multi-scale heterogeneity can be taken into account when discussing, not only single events of different magnitudes, but also a sequence of such events. The conclusion inferred from the study of Ide and Aochi (2005) on single events is that a perturbation (rupture initiation) on any small heterogeneity remains as a local event of small magnitude with a few exceptions that lead to the rupture of the entire system (a so-called characteristic event) showing a cascade-like rupture growth (Ellsworth and Beroza, 1995). Although each event is perfectly governed by the physical law, the system behavior appears stochastic because of the uncertainty of the initiation process. As emphasized in Ide and Aochi (2005), a rupture can initiate from a part much smaller than its final size and such an initiation often becomes unstable due to local fluctuations in stress or strength, which are not described in the deterministic simulation of the rupture propagation. Thus the initiation process requires a stochastic process representing unknown microscopic heterogeneities. This process is controlled by deterministically calculated macroscopic parameters, such as the average stress level. Besides the studies of earthquake dynamic rupture, there are many previous works on simulating seismicity. One end member, as represented by Otsuka (1971) and Bak and Tang (1989), for instance, is based on a simple mechanical model of stress release on a concerned grid and stress redistribution on the surrounding grid. Although these models show the characteristics of self-organized criticality, such as a wide range of events under no explicit spatial inhomogeneity, the governing system has only the nearest-neighbor interaction of a spring between two discretized blocks and may not be a proper approximation of a continuum medium where earthquakes occur. Thus another kind of mechanical model based on fracture mechanics in an elastic medium has been

developed (Mikumo and Miyatake, 1979; Yamashita, 1993; Rice, 1993; Ben-Zion and Rice, 1993; Lapusta et al., 2000; Zöller et al., 2005b; Hillers et al., 2006). As a crack evolves deterministically according to the elastic response and stress-displacement constitutive relation on the crack, the system approaches a limit cycle unless the grid resolution is insufficient with respect to a characteristic scale determined by the fault constitutive relation (Rice, 1993). In this case, some other heterogeneity in the parameters is required to generate the complexity of the seismicity in the continuum medium as in the dynamic rupture process of single events. Numerical efforts have been made to treat more complex heterogeneity and a large number of degrees of freedoms have been added to simulate a wide range of earthquakes. As we focus on the effect of dynamic earthquake events and so-called “asperities”, we will adopt a friction law that does not allow any aseismic slip during the simulation. There exist some studies, e.g. Lapusta et al. (2000) and Lapusta and Liu (2008), which simulate sequences of dynamic events and interseismic creeping within a single computational procedure and suggest that the interseismic processes may significantly change fault stress/strength conditions before earthquakes and, therefore, that it influences dynamic rupture processes. However, in most studies, smaller scales, which cannot be deterministically described on a model element, are not considered. In this case, these simulations are always deterministic regardless of the variety of event sequences. The aim of this paper is to take into account such small-scale instabilities and their consequences on macroscopic earthquake sequences.

In this paper, we first explain the concept of a multi-scale heterogeneous fault according to Ide and Aochi (2005) and propose a process of stochastic rupture initiation controlled by a temporal evolution of stress. Then we examine five different distributions of

fracture energy (fault heterogeneity maps) randomly generated according to our rules and then carry out the numerical simulation of earthquake sequences during a hundred years. Each of these sequences is physically simulated using elasto-dynamics for a rupture event. Finally we analyze the simulation results in terms of their spatio-temporal characteristics. We are interested especially in how characteristic events occur in the sequence.

2. Model

2.1 Multi-scale heterogeneous fault description

Let us consider a single isolated square fault segment under a far-field tectonic loading. Our fault model is principally based on the previous one of Ide and Aochi (2005), in which circular patches of different sizes are distributed randomly on a fault plane as illustrated in Figure 1. The number of patches follows a fractal distribution of the size-number relation. Letting N_n be the number of the patches of the *n*-th order with a radius r_n:

$$r_n = 2^n r_0 \tag{1}$$

then we set:

$$N_n = 2^{-Dn} N_0 \tag{2}$$

where the fractal dimension is chosen as $D = 2$. There are 16384 ($= N_0$) 0-th order patches of the smallest size, while one for the 7th order patch whose radius is 2^7 = 128 times larger than the smallest ones. Additionally we introduce an 8^{th}-order patch with an appearance probability of 0.25. In this paper, we call these patches and patch distribution simply as the heterogeneity and fault heterogeneity map, respectively. It

should be noted that, as explained in the later sections, no other intrinsic heterogeneity is assumed in our model, namely heterogeneity in the stress field is generated naturally according to the earthquake history and stress loading is uniform over the fault. .

Next it is assumed that each patch has fracture energy G_c proportional to its radius:

$$G_c \propto r_n \quad , \tag{3}$$

so that the smallest patches represent the weakest points. A simple slip-weakening friction law between shear stress τ and fault slip Δu is introduced to govern the rupture process on the fault during slipping:

$$\tau(\Delta u) = \Delta\tau_b(1-\Delta u / D_c)H(1-\Delta u / D_c) + \tau_r \tag{4}$$

where the parameters $\Delta\tau_b$ and D_c are called breakdown strength drop and critical slip distance and $H(\cdot)$ is the Heaviside function. τ_r represents a level of so-called dynamic friction (residual stress), but hereafter $\tau_r = 0$ is assumed without loss of generality for a planar fault problem because we discuss the deviate stress. The fault strength (static friction) is thus written as $\Delta\tau_b + \tau_r$ when the fault is not sliding. As is mentioned later, an immediate healing process is assumed. In this formulation, fracture energy is simply written by $G_c = \Delta\tau_b \cdot D_c / 2$. We assume $\Delta\tau_b$ uniform everywhere at every scale (= 5 MPa) to simplify the problem so that the scale-dependent parameter of interest is D_c. Hereafter we will discuss this parameter D_c instead of the fracture energy G_c. The importance of the linear scale dependence of D_c has been pointed out by different researchers (e.g. Andrews, 1976; Matsu'ura et al., 1992; Ohnaka, 2003). This scale dependence is a necessary condition for the self-similarity of the dynamic earthquake rupture between small and large earthquakes, which is strongly implied by

laboratory experiments and seismological analyses. The problem had been the degree of variation in D_c for a single system. Integrating the concept of Matsu'ura et al. (1992) and Ohnaka (2003) that D_c originates from the topology of fault surface, our previous work (Ide and Aochi, 2005), consisting of Equations (1) to (4), has successfully shown that various sizes of earthquakes occur on a single fault system having a D_c distribution.

In this study, the dimension of the fault area is 16.4×16.4 km^2 surrounded by an unbreakable barrier, which implies that this fault is isolated from the outside. This fault is subdivided into 4096×4096 elements which cannot currently be treated directly by our numerical scheme. Thus, as explained in the next section, we dynamically adjust the grid size of the calculation to the scale where the rupture is progressing during each earthquake. We generate five different distributions of circular patches as shown in Figure 2. The location of each patch is randomly determined within the whole fault plane. The minimum D_c is 0.25 mm. It is noted that the largest patch does not always appear as its appearance probability equals 0.25. This fault is also charged by a constant far-field tectonic loading, which controls stochastic initiation process as explained in a later section. Thus the complexity arises both from the stochastic growth of earthquake rupture and from the stochastic rupture initiation process.

2.2 Simulation of the dynamic rupture stage

In this section, we explain the part of the deterministic calculation of this simulation based on the dynamic and static response in a homogeneous, infinite elastic medium. Once rupture is initiated somewhere on the fault, we calculate the spontaneous dynamic process using a boundary integral equation method (BIEM: Fukuyama and Madariaga,

1995, 1998) and a renormalization technique (Aochi and Ide, 2004), which allows us to follow the growth process of the rupture by changing the grid size until the arrest of rupture by conserving the released seismic moment and the fracture energy on the concerned area. The rupture initiation at the initial step is given by a finite circular crack; this effect disappears rapidly after the renormalization process [See Figures 2 and 4 in Aochi and Ide (2004)]. From the viewpoint of larger scales, the dynamic rupture process appears to begin as a point in our configuration. The BIEM calculation is always carried out on the unit grid with 64×64 boundary elements by using a technique of two-dimensional fast Fourier transforms. According to the definition of the BIEM, nothing happens outside the physical model region, i.e. we do not need to consider it. An unbreakable barrier theoretically represents the condition that fault slip always equals zero.

Once a dynamic rupture begins (see the next section on how it is triggered), the stress drops in the ruptured area with fault slip according to Equation (4) while stress accumulates in the surrounding area according to elasto-dynamics, calculated by the BIEM. During this process, the fault slip is triggered at each grid point once the applied shear stress exceeds the fault strength ($\Delta\tau_b + \tau_r$). This means that there remains in principle a possibility that dynamic stress perturbation may cause a rupture at distance away from the rupture front, as our model is intrinsically heterogeneous at all scales. However, a triggered event of significant size is rarely observed in the following simulation. This is because, as we will see later, the probability for a rupture to grow logarithmically decreases with size and also because such instabilities may soon coalesce with the dominant rupture area even if it exists. Thus, although this mechanism could be important when discussing high-frequency seismic wave radiation and

dynamic triggering in a more complex fault system, its influence is limited for the macroscopic view of rupture growth on a single plane, which we aim to discuss in this paper. Once all the grids are complete at a scale where the simulation is progressing, the dynamic rupture simulation of one event finishes. At the end of each dynamic rupture simulation, we calculate the static stress change due to the event. To simplify the numerical procedure, the near-field stress change is calculated based on the scale where the rupture has terminated, while the far-field stress is rapidly calculated on the large-scale grids by using a renormalization technique. This is a good enough approximation since the detail of the slip distribution mostly perturbs the region close to the ruptured area and the change in the stress field is gradual at distance. This significantly speeds up the process.

The slip-weakening law in (4) has no healing mechanism, but it is unlikely that the ruptured area remains weak a long time after the event. For simplicity, we, therefore, assume that the fault is healed immediately after arrest, to its original strength value and that it keeps the same value of fracture energy, or D_c, resetting Δu to be zero in Equation (4). The first event occurs under a uniform stress field, but the stress field evolves to be heterogeneous through the ongoing seismicity. During the sequences, the stress values may even become negative in our numerical system due to the overshooting effect of the dynamic rupture process. However, "back slip" is prohibited, as τ_r in Equation (4) is not really zero but high enough to suppress backward motion in nature.

2.3 Stochastic initiation process and system evolution

The initiation criterion for each event is a fundamental assumption in this study. We

introduce a stochastic description reflecting unknown heterogeneity and a macroscopic stress field, which is the available information in the above framework. Laboratory experiments suggest a Weibull-type distribution for the strength distribution of rock material (e.g. Yamaguchi and Nishimatsu, 1967) and previous numerical studies adopted such a strength distribution (e.g. Mikumo and Miyatake, 1978, 1979). However, this study assumes uniform fault strength and introduces prescribed fracture energy at each point on the fault as the rupture process is deterministically described by a fault constitutive relation and elasto-dynamics. Thus, we need another way to model the fragility of each point with respect to the given fracture criterion and stress condition.

As shown in numerous deterministic simulations, giving a small instability to a nucleation area with some finite size allows spontaneous dynamic rupture propagation even if the stress is moderately loaded on the fault system. This is often discussed by some normalized parameter between stress, strength or fracture energy (e.g. Das and Aki, 1977; Shibazaki and Matsu'ura, 1998; Madariaga and Olsen, 2000). These all imply that there remains an arbitrary selection of the nucleation points with respect to the stress field and it is well known that this significantly affects the rupture history and the wave radiation (e.g. Guaterri et al., 2003; Aochi et al., 2006). No quantitative description of the selection of such an initiation process has been established, as this may be physically related to the microscopic heterogeneity that we cannot describe deterministically. In this paper, we thus assume that this selection is stochastic with a function of accumulated stress and propose to approximate it by a Weibull distribution function. The selection, i.e. the probability of rupture P of any patch of the minimum size under the applied stress τ within a fixed duration, is written using a Weibull distribution:

$$P(\tau;k,\lambda) \propto (k/\lambda)(\tau/\lambda)^{k-1} exp(-(\tau/\lambda)^{k}), \quad (5)$$

where k (shape parameter) and λ (scale parameter) determine the shape of the distribution and the characteristic stress level related to the maximum probability, respectively. This probability P is defined to be zero when $\tau \leq 0$ and a condition of $\tau > 5$ does not exist in our context. Equation (5) might be replaced by another functional form, but the merit of using this function is that it is sufficient to study k since λ is taken equal to the assumed peak strength (λ = 5 MPa). Figure 3 shows this function for different values of k. This qualitatively matches our hypothesis, where the probability is effectively zero at very low stresses and increases with the external stress until the supposed strength. A large value of k produces a narrow peak around λ, which makes rupture initiation sensitive to the macroscopic stress concentration. In contrast, with a small k, rupture initiation under low stress is more likely, which means that the microscopic stress perturbation on any patch is relatively independent of the initiation probability that is controlled mainly by surrounding macroscopic stress field.

In the presence of tectonic loading, stress state and the probability of event occurrence depends on time. Adjusting the far field stress loading rate, we may control the recurrence time of seismic cycles. Event frequency is related to Equation (5). To normalize this equation in a seismic cycle, we suppose a roughly characteristic event of this fault (Mw about 6) every T year. The standard Gutenberg-Richter law then predicts $10^{(6-M)}$ events of magnitudes greater than M during the period T. Remembering that the minimum simulated event appears around magnitude M = 1 corresponding the smallest patches on the fault system, we assume that all the initiation points are triggered at least once during these T years. The average event interval is

then t_{int} = T (years)/16384 (events), and the mean probability of events is P_{event} = t_{int}^{-1} per unit time. Namely we normalize Equation (5) so as to satisfy the following relation taking a stress value of 3MPa as reference:

$$N_{min} \times P(\tau = 3 \text{ MPa}; k, \lambda) = P_{event}. \quad (6)$$

However, this normalization is based on the assumption of a uniform stress field of 3 MPa. As we will see in the following sections, stress field evolves with tectonic loading and event sequences and hence the stress applied on the system is not stationary. More precisely, it is lower during most of the period because the characteristic events release the entire accumulated stress at once. As a consequence, we will see that the simulated seismicity is much lower than expected. We finally assume that the tectonic stress loading for each time step, $\Delta\tau_{tectonic}$, is constant, namely stress builds up to 3 MPa, taken as the reference above, during T. The parameters are summarized in Table 1.

We note that the above procedure selects either no hypocenter or one hypocenter at each time step. If no hypocenter is selected, we advance in time. If one hypocenter is selected, this defines the initial model space at the finest scale where we begin a dynamic simulation. In the dynamic rupture simulations, an instantaneous strength drop is given at the beginning on a small area within a selected smallest patch. Namely the strength is forced to be zero in Equation (4). Once selected, this initial process has a positive stress drop so that the rupture progresses more or less spontaneously according to the current boundary conditions.

3. Simulation results

We execute the simulations for five different fault heterogeneity maps (Figure 2) based on the above procedure. The parameters are given in Table 1, considering a tectonically active zone (on average a M6.5 event every 20 years). The parameters of the Weibull's function are chosen after studying the results of our preliminary run. We discuss the sensitivity to the parameters in a later section. We begin the simulation with a uniform stress of 3.5 MPa expecting the first characteristic earthquake to occur early in all the simulation; this warming-up period (cycle 0) is not taken into account in subsequency discussions. Here the characteristic earthquake is defined as the rupture process propagating on the whole fault area and being stopped by the barriers outside of the modeled region. Such an event completely releases the accumulated stress on the fault. We run each simulation for a hundred years, by running the stochastic initiation process every hour and by simulating the dynamic rupture process for a time step for a minimum 0.33 ms. This takes more than a week on a quad-core machine, although one earthquake is usually simulated within a few minutes. In the following section, we first discuss the statistical aspects of the earthquake sequences and then watch the details of the rupture process occurring in the simulation, from deterministic point of view.

3.1 Earthquake sequences with time

Figures 4 and 5 show the earthquake sequences with time for a hundred years for five fault heterogeneity maps. Characteristic events (Mw 6.4-6.5) repeat constantly in all cases with an average recurrence interval of about 20 years after a certain number of earthquakes have occurred. As reported in Table 2, the variation in the recurrence

interval of characteristic earthquakes is relatively small. The difference between maximum and minimum recurrence times within each simulation is less than 5 % of the average recurrence time for maps (1) to (3), and 7 % and 13 % for (4) and (5), respectively. This originates from the internal effect of the stochastic rupture initiation, including the choice of random numbers and the subsequent earthquake histories along the fault. More interestingly, the maximum difference in the average recurrence time according to the fault heterogeneity maps is rather large, 1.89 years, namely the diversity due to the maps is larger than the fluctuation (randomness) within each simulation except for (5). This indicates the importance of the geometrical distribution of the patches (fault heterogeneity), although all the maps are realizations of the same statistical model. The uniqueness of (5) is clear in the fault heterogeneity map where the maximum patch is accidentally missed.

It is found that the number of earthquakes accelerates with time and the maximum magnitude also increases. This is controlled by the external stress level. First, the increase of stress level raises the probability of the rupture initiation following Equation (5) so that it eases the appearance of earthquakes with time. On the other hand, the dominance of large events indicates that larger earthquakes require higher stress loading over a large area, while small earthquakes can occur within a localized stress accumulation. Higher background stress enhances patch interaction and growth to become a large event.

It is not surprising that no earthquake appears just after a characteristic event. This is because the stress is completely released across the entire fault and it takes time to recover enough stress to lead to a new earthquake. This is a common feature in previous studies, which do not introduce any specific mechanisms for delayed rupture, relaxation

of the medium, pore fluid flow and so on (e.g. Zöller et al., 2005a).

3.2 Earthquake size distribution

In this section, we report the size distribution of the earthquakes. As already clearly shown in Figure 4, the greater tectonic stress accumulated with time, the larger the earthquake that appears. This indicates that the larger earthquakes require widely accumulated stress. On other hand, small earthquakes easily occur at any time without growing to large events, mainly because they are controlled by small-scale heterogeneities that are recovered relatively quickly. Figure 6 shows the size-frequency relation for the cumulative number of earthquakes within each simulation. The characteristic events of around M6.5 are shifted from the scaling relation of smaller earthquakes. We then find that most of the seismic cycles in all the simulations briefly show a linear Gutenberg-Richter relation, while the ones of simulation (4) and (5) show significantly curved relations with dominant magnitudes around 3 [there is also a small curvature in the relation for simulation (3)]. In the latter case, it should be noted that the number of earthquakes also increases. This means that there should be something characteristic at this scale to break the scaling relation. Many earthquakes cannot grow larger than this size. This feature can be understood deterministically by detailed analysis of the earthquake sequences (See section 3.4)

The absence of aftershocks has already been reported in Figures 4 and 5. In nature, the characteristic event accompanies many aftershocks, which often show a Gutenberg-Richter size-frequency relation. On the other hand, it is also known that such relations are visible in any time period during a seismic cycle, even for background

seismicity. Therefore it is not surprising that a Gutenberg-Richter behavior appears without aftershocks.

3.3 Spatial pattern of sequences

The spatial patterns of seismicity in Figure 7 have some interesting features. First, although the seismicity is greatly distributed, some concentrations and/or gaps are found. From the macroscopic view of the whole fault area, the seismicity is located more on the upper section of the fault in (1) and (2) and located on the lower section in (3), for example. On the other hand, in some cycles such as indicated in green for (4) and purple for (5), the sequences sometimes leave a gap in certain areas and in the surrounding regions many more earthquakes are found. In this case, the number of earthquakes also increases (Figure 5) and some dominant earthquake size appears (Figure 6). Both phenomena should be the result of some physical process of earthquake ruptures regardless of the randomness of the rupture initiation. On the other hand, we find that the hypocenters of the characteristic earthquakes are sometimes close to one other, as four events in (1) and all events in (2), for example. In (3), the hypocenters are divided into two different areas. We will next discuss these similarities and the complexity by considering in detail the process of earthquake ruptures.

3.4 Stress field evolution

The upper and lower rows of Figure 8 respectively show the stress field before and after every characteristic earthquake in the simulations. More exactly, the upper row

represents the final stress of the precedent earthquake and the lower row is the final stress when the characteristic earthquakes have finished. The evolution of the stress field pattern can be classified into two groups: rather homogeneous evolution represented by (1) and (2) of Figure 8, and inhomogeneous evolution due to some visible ruptured area of intermediate magnitude earthquakes, especially observed in the third cycle of (4), for example. Comparing Figure 8 with the fault heterogeneity and seismicity (Figures 2 and 7), we can find how each system becomes ready to rupture the whole area, or the largest patch. Such instability requires some large areas with almost complete stress drop. These areas may be formed dynamically within a single event as a cascade, which we may call dynamic nucleation, or it may happen during many precedent earthquakes as in a quasi-static nucleation.

The fault heterogeneity maps (1) and (2) (Figure 2) are typical examples of the former case. Namely the patch distribution allows a cascade-like rupture growth from the smallest patch to the largest one (Ide and Aochi, 2005). A small perturbation can easily grow to a characteristic event without a large quasi-static nucleation area. Only a small number of earthquakes occur leaving a clear gap between magnitude 4 and 6.5 in the magnitude-frequency relation. This also explains the closeness of the hypocenters of the characteristic events. In map (1), a cascade-like growth must propagate into the largest patch located in the right upper corner. The only exception is a rupture that begins far from this patch at the end of the first cycle (star in purple in Figure 7), the rupture process takes longer, by about 40 %, to propagate along the whole fault area, than in the other simulations. Despite the similarity of the initial scenario, slightly different behavior can be observed for the characteristic event. The rupture may initiate from a different direction with respect to the largest patches, as observed in the Parkfield

earthquakes in 1966 and 2004 (Bakun et al., 2005; Murray and Langbein, 2006). After the rupture of the largest patch, every rupture similarly propagates unilaterally to the lower part. The rupture directivity towards the bottom releases much stress at the bottom with respect to the top, which is known as the overshoot effect. This effect explains low seismicity in the lower part of the fault and precludes preparation to a characteristic event.

In contrast, large quasi-static nucleation areas with low stress appear before some characteristic events for maps (4) and (5) in Figure 8. In other words, this is a pre-slipped area and the stress concentration surrounding this area promotes the initiation of a large earthquake. The typical case is clearly seen in the third cycle of map (4). Here an earthquake of magnitude 5.7 occurs in early stage of the stress build-up (Figure 4) and this cannot grow further at this time. The seismicity in and around the ruptured area becomes high (Figure 7). In other words, the characteristic earthquake fails to occur following one favorable scenario and the system has to wait a long time for the next possible scenario (see the third characteristic earthquakes) when the system is highly charged and heterogeneous. This increases the seismicity (Figures 5 and 6), especially small earthquakes occurring in the surrounding area, which cannot become large enough to lead to a characteristic event (Figure 7). These are anomalies in the fault system, controlled by the timing of an intermediate earthquake.

Map (3) in Figure 8 shows similar characteristics to maps (1) and (2) although it has a slightly nonlinear G-R relation (Figure 6). The characteristic events always begin on the largest patch without interacting with the other large patches located in the middle-to-upper part. This means the coalescence of the smaller patches (light blue) is strong enough to break the largest ones. Another reason comes from the fact that the

patches in the upper part are not activated so favorably due to the directivity effect of the characteristic earthquake once this occurred on the lower part.

In this way, the anomalies found in the simulations can be understood while analyzing in detail the on-going earthquake sequence through the statistical features and the physical rupture processes. Therefore the scenario of the forth-coming characteristic earthquake in the concerned seismic cycle can be constrained with respect to its time, position and rupture directivity.

4. Discussion

We have observed that different heterogeneity maps with the same statistical features lead to a diversity of earthquake sequences, conserving some deterministic features of the characteristic earthquakes. Let us now consider the sensitivity to the parameters of the assumed rupture initiation process. The form of our probabilistic function (5) is hypothetical and the shape parameter k controls the sensitivity of initial rupture process to the loaded stress field, as demonstrated in Figure 3,. For easy comparison, we use the same maps as (1).

First Figure 9 shows a case for $k = 3$ (Figure 3), where the earthquake initiation point is selected almost independently with respect to the stress distribution determined by the previous earthquake history. Therefore the earthquake distribution always remains almost uniform without any explicit localization (d). As a result, the number of smaller earthquakes increases in the size-frequency relation (Figure 9b-c).

Figure 10 shows the opposite case, $k = 60$, where rupture selectively starts from a patch of high stress accumulation and system behavior is significantly different. Since the

computation takes too long, we show only the first year starting with a uniform stress condition, which represents a typical behavior of this system. Very early earthquakes are dispersed over the fault, as the initial stress is uniform anywhere. However, soon the predominant earthquake sequence appears (bottom part of Figure 10d), where the following earthquakes occur only near the periphery of the previous rupture area. In the rest of the model space, the initiation probability (Figure 3) remains very low. This predominant sequence progresses very quickly, as earthquakes are triggered at almost every time step. Thus, the sequence shows a very concentrated time history, as seen in Figures 10(a) and (b), suggesting insufficient temporal resolution with the current time step. The extension of the ruptured area works as the quasi-static nucleation process and the characteristic earthquake occurs after the ruptured area becomes a critical size. The earthquake size distribution deviates from self-similar relation. In this example, the heterogeneous stress field generated rapidly by some initial earthquakes controls the following sequence. It also suggests that any anomaly in the initial stress field may control the whole earthquake sequence.

It is widely known that some cellular automaton models generate a Gutenberg-Richter like size-frequency distribution (e.g. Bak and Tang, 1989), while elastic continuum models with a characteristic length converge into a periodic behavior (e.g. Rice, 1993). Our system behavior cannot be interpreted using these two end members. Figure 9 and 10 show that stochastic initiation process must be adjusted to mimic the vast distribution of the seismicity, characteristic earthquakes, and a Gutenberg-Richter relation. However, the essential part of our model is the heterogeneity map derived from Equations (1) – (3), as randomly initiated rupture on such a heterogeneous map gives a Gutenberg-Richter relation (Ide and Aochi, 2005) even without any system evolution.

As the introduction of system evolution sometimes interferes with the intrinsic features of the system, anomalies found in the current simulation might be hidden if we consider further complexity of the natural system.

Our general concern for natural earthquakes is how a characteristic earthquake appears in the seismic cycle. We assume built-in heterogeneous D_c distribution that is conserved after each characteristic event, which might be debatable. Probably the patches (fault heterogeneity) at larger scales is intrinsic (invariable in space) during a few seismic cycles, as inferred from the slip distributions of subsequent earthquakes in the subduction zones around Japan (Nagai et al. 2001, Yamanaka and Kikuchi, 2003) and at Parkfield (Murray and Langbein, 2006). In laboratory experiments, large asperities due to geometric irregularities are well conserved such that ruptures begin on the faults similarly (Ohnaka and Shen, 1999) and this matches with our initial model of multi-scale D_c (Ide and Aochi, 2005). As the initiation process at smaller scales in our simulation is stochastic, the earthquake sequences appearing at small scales seem different every time. Keeping the same heterogeneity at all scales may be acceptable as a first attempt. However, this point should be discussed further in future studies.

As mentioned earlier, the stochastic rupture initiation process can be debated because most of our observations concern the macroscopic fracture criterion. Without knowledge of the real dynamics and fine-scale heterogeneity in the first instability scale, such a stochastic description would be a practical substitute. Then, our current normalization process homogenizes the initial field information during the rupture propagation. This is correct at the scale of characteristic earthquakes, but it will be another interesting topic to study how smaller heterogeneity influences the rupture

process at each scale. Fine-scale complexity around the rupture front may generate very complex seismic wave radiation at high frequencies. Such processes will require further numerical developments, such as auto-adopted gridding within the BIEM.

5. Summary

A sequence of complex dynamic rupture events under a constant tectonic loading is simulated based on a multi-scale heterogeneous fault model with circular patches, a stochastic rupture initiation process governed by a Weibull probabilistic function and instantaneous healing of the fault strength by keeping the same map during every cycle. The simulation results are analyzed statistically to explain their diversity and their similarity both from the statistics of the seismicity and from the physical process of the earthquake rupture. As previously shown in Ide and Aochi (2005), a self-organized system such as the Gutenberg-Richter size distribution relation originates from the multi-scale heterogeneity map we assume. However, different simulations show that the history of stress field may hide this intrinsic feature. The diversity of earthquake sequences is principally controlled by the spatial distribution of the patches. Although the exact time and position of the onset of the characteristic earthquakes cannot be predicted, they occur rather regularly in time and similarly in different seismic cycles. Dynamic rupture processes of the characteristic earthquakes leave heterogeneous residual stresses due to directivity and overshoot effects, so that this pattern often controls the spatial distribution of the following seismicity. It is also found that larger earthquakes may occur later in each seismic cycle. This means much stress concentration over large area is required for a rupture to propagate spontaneously to a

larger area. Some irregular characteristic earthquakes may occur based on the map and the randomness of the preceding earthquake sequence. In this case, an anomaly in the seismicity such as the number of earthquakes, size distribution and spatial distribution becomes visible. From the physical viewpoint, this is due to an intermediate earthquake before the stress is sufficiently accumulated over the fault system. This means that such an anomaly is not predicable before the cycle, but understandable through the analysis of the concerned earthquakes during the cycle. In nature no fault system can be isolated from the others, so that the phenomena should be more complex. However, the similarity and the diversity simulated in this study, governed by the structure of an inherent distribution of D_c, suggests the importance of pre-existing fault heterogeneity structure for the appearance of earthquake sequences, including those that are characteristic.

Acknowledgments

We thank Martin Mai, Sandy Steacy and a few anonymous reviewers for their critical comments on our manuscript. Some of them encouraged us to test different heterogeneous maps to improve our comprehension and discussion. We also thank John Douglas for reviewing our revised manuscript. H.A. receives partial financial support from the French national project INSU 3F - Rhéologie des asperities de faille (2007). The parallel calculations were carried out in the Digital Information Systems Division of the BRGM. This study is a contribution to BRGM's research program on seismic risk. This work is also partially supported by Ministry of Education, Culture, Sports, Science and Technology (MEXT), Japan.

References

1. Andrews, D. J. (1976), Rupture propagation with finite stress in antiplane strain, *J. Geophys. Res.*, 81, 3575-3582.
2. Andrews, D. J. (2005), Rupture dynamics with energy loss outside the slip zone, J. Geophys. Res., 110, doi:10.1029/2004JB003191.
3. Aochi, H. and E. Fukuyama (2002), Three-dimensional nonplanar simulation of the 1992 Landers earthquake, J. Geophys. Res., 107, doi:10.1029/2000JB000061.
4. Aochi, H. and S. Ide (2004), Numerical study on multi-scaling earthquake rupture, *Geophys. Res. Lett.*, 31, L02606, doi:10.1029/2003GL018708.
5. Aochi, H., M. Cushing, O. Scotti, and C. Berge-Thierry (2006), Estimating rupture scenario likelihood based on dynamic rupture simulations: the example of the segmented Middle Durance fault, southeastern France, *Geophys. J. Int.*, 165, 436-446.
6. Atkinson, B. K. (1984), Subcritical crack growth in geological materials, J. Geophys. Res., 89(B6), 4077-4114.
7. Bak, P. and C. Tang (1989), Earthquakes as a self-organized critical phenomenon, J. Geophys. Res., 94, 15635-15637.
8. Bakun, W. H., B. Aagaard, B. Dost, W. L. Ellsworth, J. L. Hardebeck, R. A. Harris, C. Ji, M. J. S. Johnston, J. Langbein, J. J. Lienkaemper, A. J. Michael, J. R. Murray, R. M. Nadeau, P. A. Reasenberg, M. S. Reichle, E. A. Roeloffs, A. Shakal, R. W. Simpson, and F. Waldhauser (2005), Implications for prediction and hazard assessment from the 2004 Parkfield earthquake, *Nature*, 437, 969-974.

9. Ben-Zion, Y. and J. R. Rice (1993), Earthquake failure sequences along a cellular fault zone in a 3-dimensional elastic solid containing asperity and nonasperity regions, J. Geophys. Res., 98, 14109-14131.
10. Beroza, G. and P. Spudich (1988), Linearized inversion for fault rupture behavior: Application to the 1984 Morgan Hill, California, earthquake, J. Geophys. Res., 93, 6275-6296.
11. Das, S. and K. Aki (1977), A numerical study of two-dimensional spontaneous rupture propagation, Geophys. J. R. Astron. Soc., 50, 643-668.
12. Duan, B. and D. D. Oglesby (2005), Multicycle dynamics of nonplanar strike-slip faults, *J. Geophys. Res.*, 110, B03304, doi:10.1029/2004JB003298.
13. Ellsworth, W. L. and G. C. Beroza (1995), Seismic evidence for an earthquake nucleation phase, Science, 268, 851-855.
14. Guatteri, M., P. M. Mai, G. C. Beroza and J. Boatwright (2003), Strong-ground motion prediction from stochastic-dynamic source models, Bull. Seism. Soc. Am., 93, pp301-313.
15. Hillers, G., Y. Ben-Zion and P. M. Mai (2006), Seismicity on a fault controlled by rate- and state-dependent friction with spatial variations of the critical slip distance, J. Geophys. Res., 111, doi:10.1029/2005JB003859.
16. Ide, S. (2002), Estimation of radiated energy of finite-source earthquake models, Bull. Seismol. Soc. Am. 92, 2294-3005.
17. Ide, S. and H. Aochi (2005), Earthquakes as multiscale dynamic ruptures with heterogeneous fracture surface energy, *J. Geophys. Res.*, *110*, B11303, doi:10.1029/2004JB003591.
18. Ide, S. and G. C. Beroza (2001), Does apparent stress vary with earthquake size?,

Geophys. Res. Lett., 28, 3349-3352.

19. Fukuyama, E. and R. Madariaga (1998), Rupture dynamics of a planar fault in a 3D elastic medium: Rate- and slip-weakening friction, *Bull. Seismol. Soc. Am.*, *8*8, 1-17.

20. Fukuyama, E. and R. Madariaga (1995), Integral equation method for plane crack with arbitrary shape in 3D elastic medium, Bull. Seismol. Soc. Am., 85, 614-628.

21. Lapusta, N. and Y. Liu (2008), 3D boundary-integral modeling of spontaneous earthquake sequences and aseismic slip, in press, J. Geophys. Res.

22. Lapusta, N., J. R. Rice, Y. Ben-Zion and G. Zheng (2000), Elastodynamic analysis for slow tectonic loading with spontaneous rupture episodes on faults with rate- and state-dependent friction, J. Geophys. Res., 105, 23765-23789.

23. Madariaga, R. and K. B. Olsen (2000), Criticality of rupture dynamics in 3D, Pure Appl. Geophys., 157, 1981-2001.

24. Mai, P. M., P. Somerville, A. Pitarka, L. Dalguer, S. Song, G. Beroza, H. Miyake and K. Irikura (2006), On scaling of fracture energy and stress drop in dynamic rupture models : Consequences for near-source ground motions, in Earthquake : Radiated energy and the physics of faulting, Geophysical Monograph Series 170, 283-293.

25. Mikumo, T. and T. Miyatake (1983), Numerical modeling of space and time variations of seismic activity before major earthquakes, Geophys. J. R. astr. Soc., 74, 559-583.

26. Mikumo, T. and T. Miyatake (1979), Earthquake sequences on a frictional fault model with non-uniform strengths and relaxation times, Geophys. J. R. Astr.

Soc., 59, 497-522.

27. Mikumo, T. And T. Miyatake (1978), Dynamic rupture process on a three-dimensional fault with non-uniform frictions and near-field seismic waves, Geophys. J. R. Astr. Soc., 54, 417-438.

28. Murray, J. and J. Langbein (2006), Slip on the San Andreas Fault at Parkfield, California, over Two Earthquake Cycles, and the Implications for Seismic Hazard, Bull. Seismol. Soc. Am., 96, S283-S303.

29. Nagai, R., M. Kikuchi, and Y. Yamanaka (2001), Comparative study on the source process of recurrent large earthquakes in Sanriku-oki region: the 1968 Tokachi-oki earthquake and the 1994 Sanriku-oki earthquake, *Zishin*, 54, 267-280 (in Japanese with English abstract).

30. Oglesby, D. D. and S. M. Day (2002), Stochastic fault stress: Implications for fault dynamics and ground motion, Bull. Seism. Soc. Am., 92, 3022-3041.

31. Olsen, K. B., R. Madariaga and R. J. Archuleta (1997), Three-dimensional dynamic simulation of the 1992 Landers earthquake, Science, 278, 834-838.

32. Ohnaka, M. and L. Shen (1999), Scaling of the shear rupture process from nucleation to dynamic propagation: Implications of geometric irregularity of the rupturing surfaces, J. Geophys. Res., 104(B1), 817-844.

33. Otsuka, M. (1971), A simulation earthquake occurrence Part 1, A mechanical model, J. Seis. Soc. Jpn, 24, 13-25.

34. Ripperger, J., J. P. Ampuero, P. M. Mai and D. Giardini (2007), Earthquake source characteristics from dynamic rupture with constrained stochastic fault stress, J. Geophys. Res., 112, doi:10.1029/2006JB004515.

35. Rice, J. R. (1993), Spatio-temporal Complexity of Slip on a Fault, J. Geophys.

Res., 98, 9885-9907.

36. Shaw, B. E. and J. H. Dieterich (2007), Probabilities for jumping fault segment stopovers, Geophys. Res. Lett., 34, L01307, doi:1029/2006GL027980.
37. Shibazaki, B. and M. Matsu'ura (1998), Transition process from nucleation to high-speed rupture propagation: scaling from stick-slip experiments to natural earthquakes, Geophys. J. Int., 132, 14-30.
38. Uchide, T. and S. Ide (2007), Development of multiscale slip inversion method and its application to the 2004 mid-Niigata Prefecture earthquake, J. Geophys. Res., 112, B06313, doi:10.1029/2006JB004528.
39. Yamaguchi, Y. and U. Nishimatsu (1967), Introduction to rock mechanics, Tokyo University Press (in Japanese).
40. Yamanaka, Y. and M. Kikuchi (2003), Source processes of the recurrent Tokachi-oki earthquake on September 26, 2003, inferred from teleseismic body waves, *Earth Planets Space*, 55, e21–e24.
41. Yamashita, T. (1993), Application of fracture mechanics to the simulation of seismicity and recurrence of characteristic earthquakes on a fault, J. Geophys. Res., 98, 12019-12032.
42. Yamashita, T. and E. Fukuyama (1996), Apparent critical slip displacement caused by the existence of a fault zone, Geophys. J. Int., 125, 459-472.
43. Zöller, G., S. Hainzl, M. Holschneider and Y. Ben-Zion (2005a), Aftershocks resulting from creeping sections in a heterogeneous fault, Geophys. Res., Lett., 32, doi:10.1029/2004GL021871.
44. Zöller, G., M. Holschneider and Y. Ben-Zion (2005b), The role of heterogeneity as a tuning parameter of earthquake dynamics, Pure Appl. Geophys., 162,

1027-1049.

Parameter	Quantity
Rigidity	32.4 Gpa
P-wave velocity	6000 m/s
S-wave velocity	3464 m/s
BIEM grid size	4 m at minimum
BIEM time step	0.33 ms at minimum
Peak strength $\Delta\tau_b$	5 MPa
Critical slip distance D_c	Variable (See Figure 2)
Weibull's shape parameter k	15
Weibull's scale parameter λ	5 MPa
Period T	20 years
Event probability P_{event}	0.1 per hour
Tectonic loading $\Delta\tau_{tectonic}$	10 Pa per hour

Table 1: Model parameters used in the simulations.

Fault Heterogeneity Map	(1)	(2)	(3)	(4)	(5)	Max (Tr)	Min (Tr)	Max(Tr)-Min(Tr)
Average Recurrence Time :Tr(yr)	19.61	20.12	20.92	21.07	19.18	21.07	19.18	1.89
Max (Tr)	19.99	20.25	21.34	21.88	21.10			
Min (Tr)	19.05	19.85	20.36	20.41	18.58			
Max(Tr)-Min(Tr)	0.94	0.40	0.98	1.46	2.52			

Table 2: Recurrence time of the simulated characteristic earthquakes for each fault heterogeneity map. To the bottom, the maximum, the minimum and their difference are presented for each map. To the right, the maximum, the minimum and the difference are calculated for the averages of each simulation.

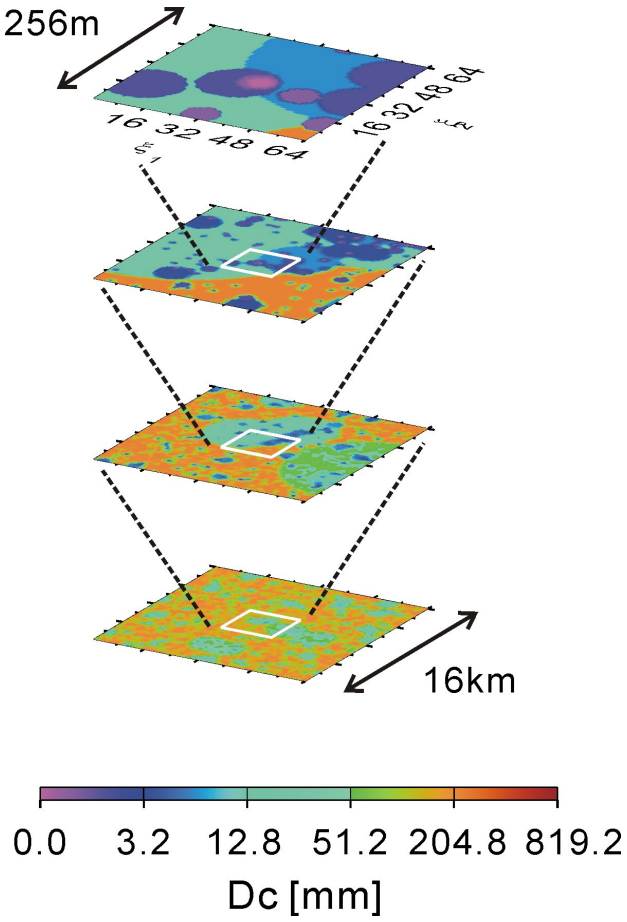

Figure 1. Schematic illustration of multi-scale heterogeneous D_c distribution [after Ide and Aochi (2005)]. Focusing on the microscopic scale, one finds numerous small parts of small D_c.

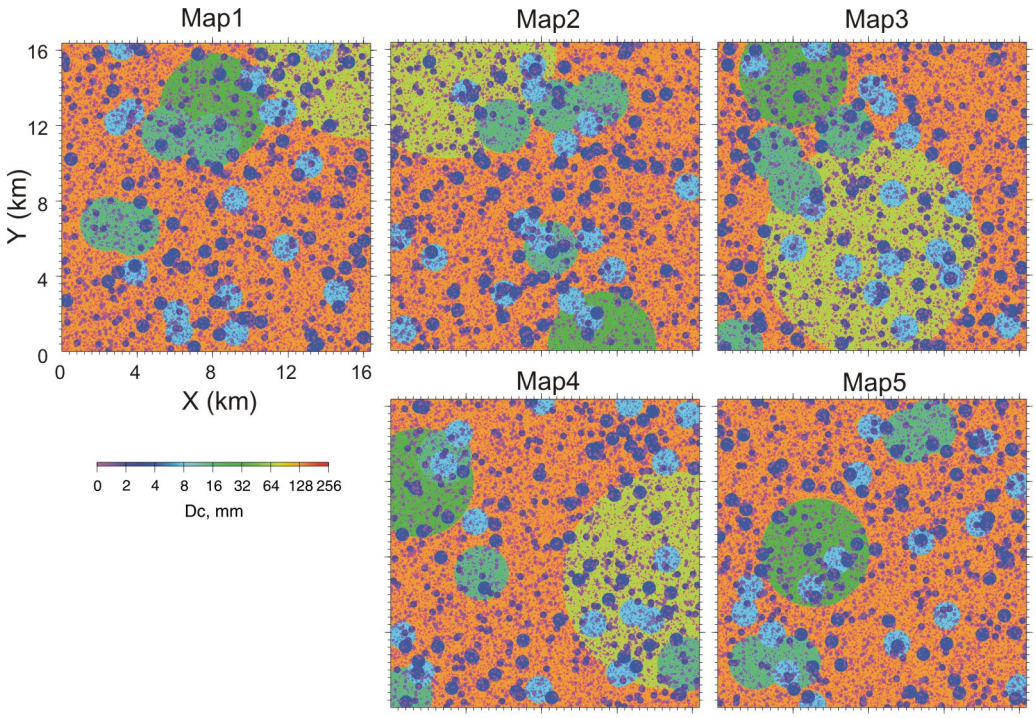

Figure 2: Five heterogeneity maps stochastically generated according to the same rules. The model area (X, Y) has a dimension of 16384 m x 16384 m, namely 4096 x 4096 grids in the minimum scale. The appearance probability of the maximum patch (olive) is 0.25, so that it is possible that this patch does not appear in the area as in Map 5. See the text in the detail.

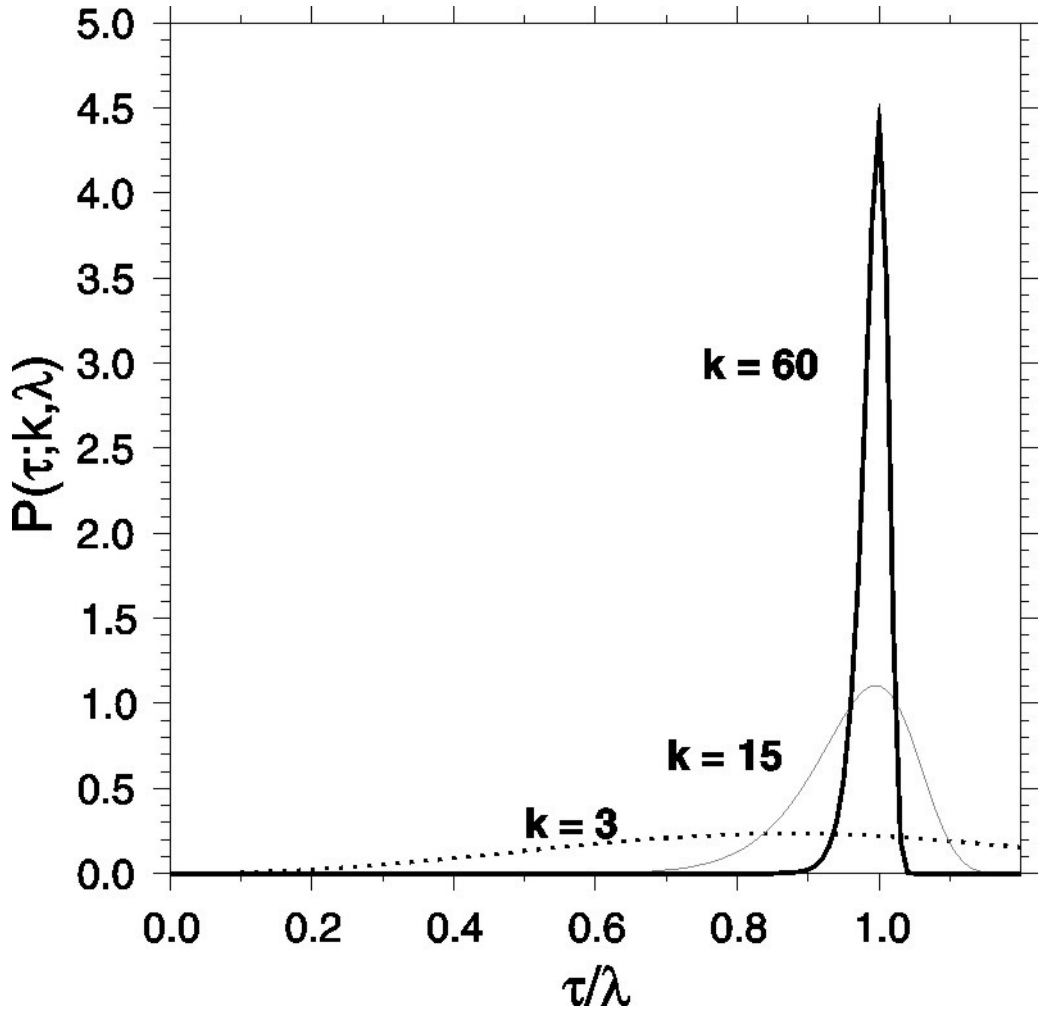

Figure 3: Probabilistic function defined by Equation (5) for k = 3, 15 and 60.

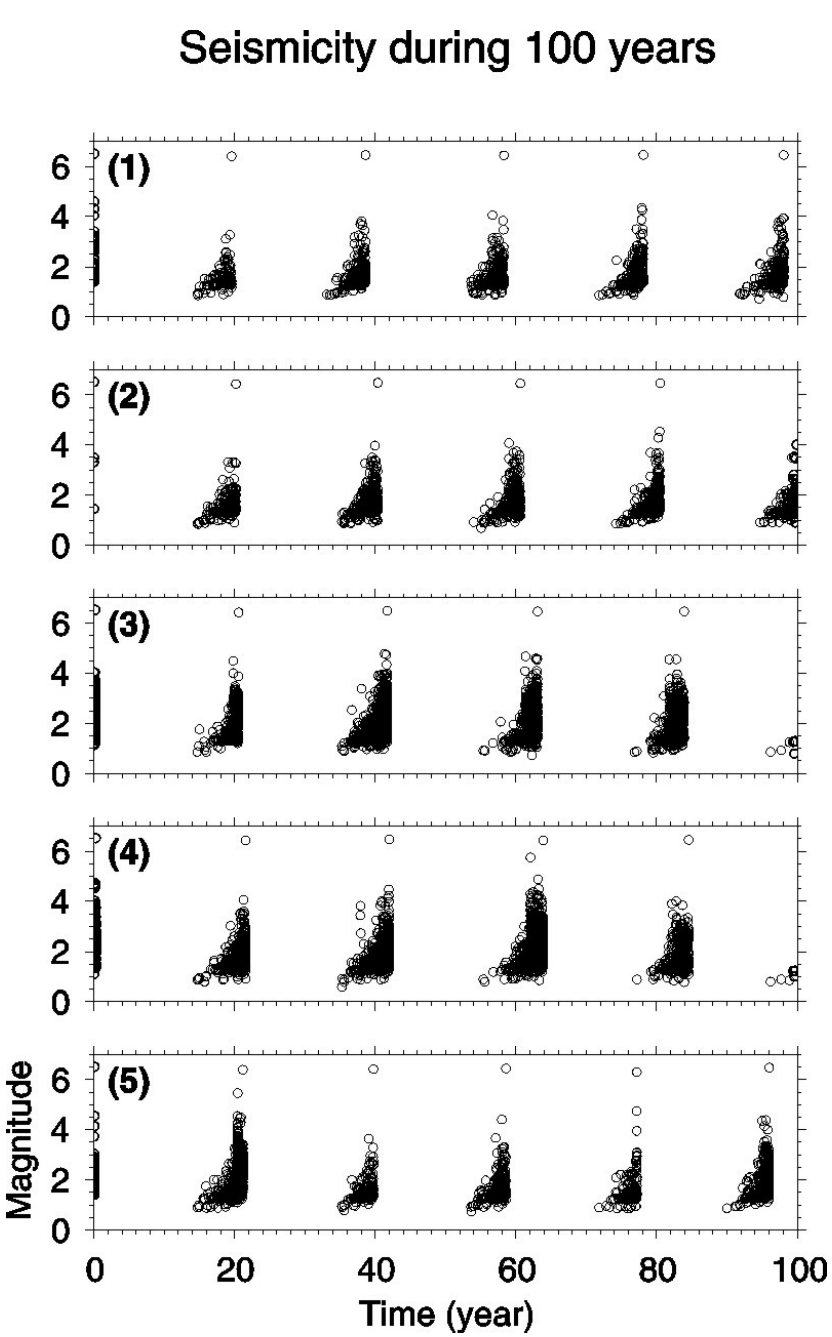

Figure 4: Earthquake sequences with time for each heterogeneity map. The number in the upper left corner corresponds to the number of each map.

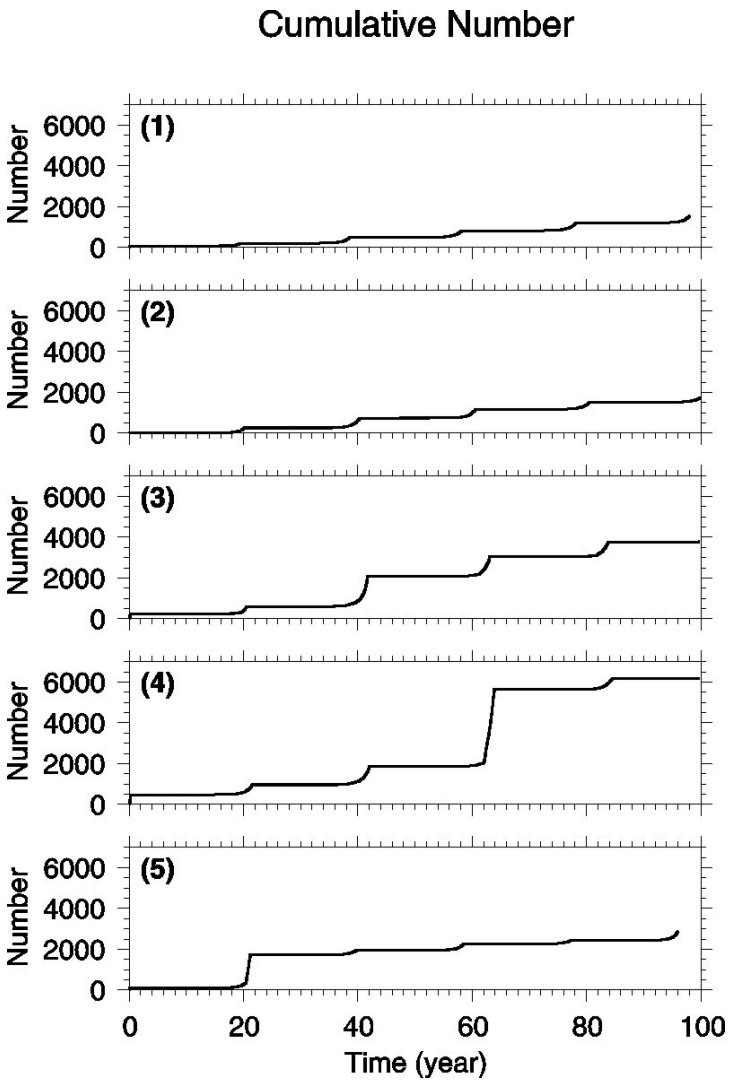

Figure5: Cumulative number of earthquakes with time for each map, (1) to (5). The curves in (1) and (5) end just before 100 years, because there is no seismicity following the previous characteristic earthquakes.

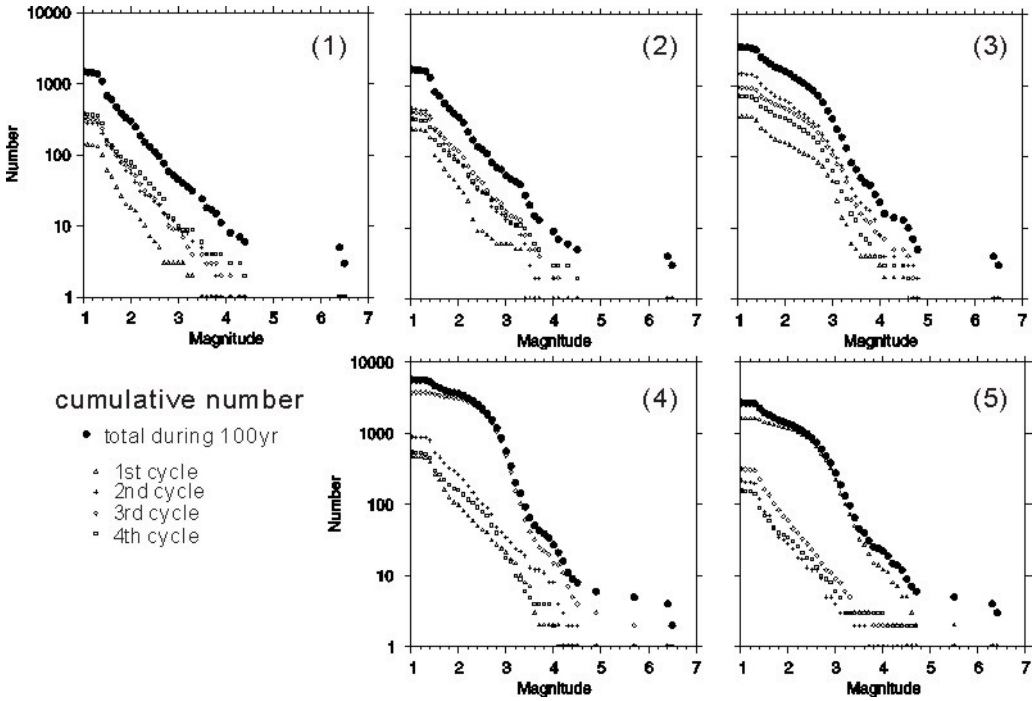

Figure 6: Earthquake numbers against magnitude for each map from (1) to (5). The black circle shows the total seismicity during 100 years of each simulation. Other marks represent four cycles within the 100 years.

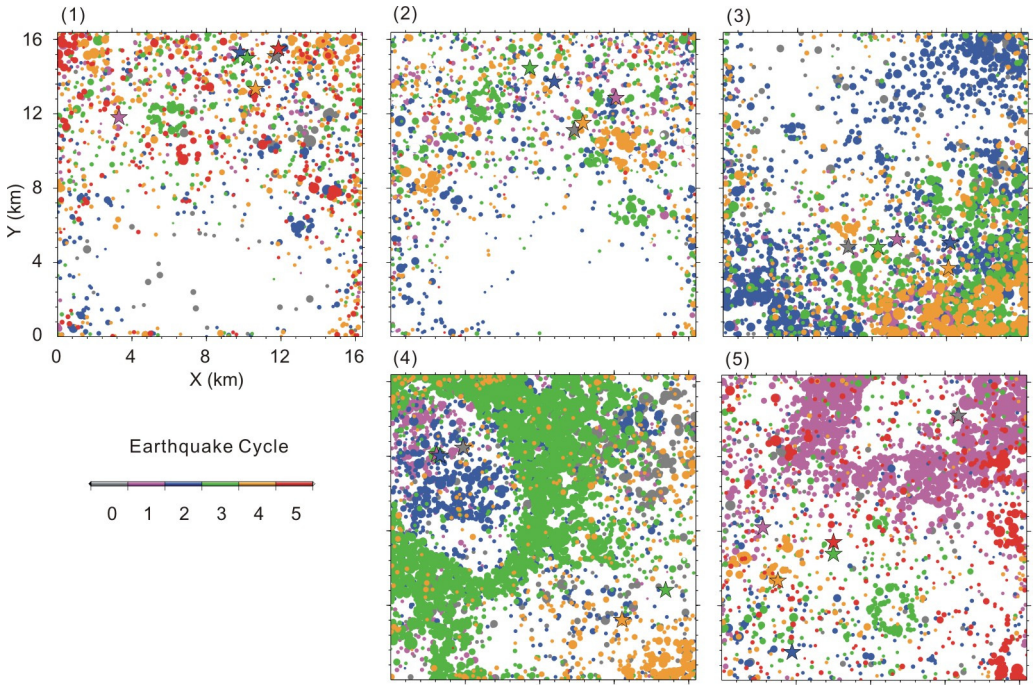

Figure 7: Spatial distribution of hypocenters of earthquake sequences during the simulated 100 years. Events are plotted by different colors according to the seismic cycles, each of which ends with the characteristic event represented by stars. The size of circles is proportional to the event magnitude, but it does not represent the physically ruptured area.

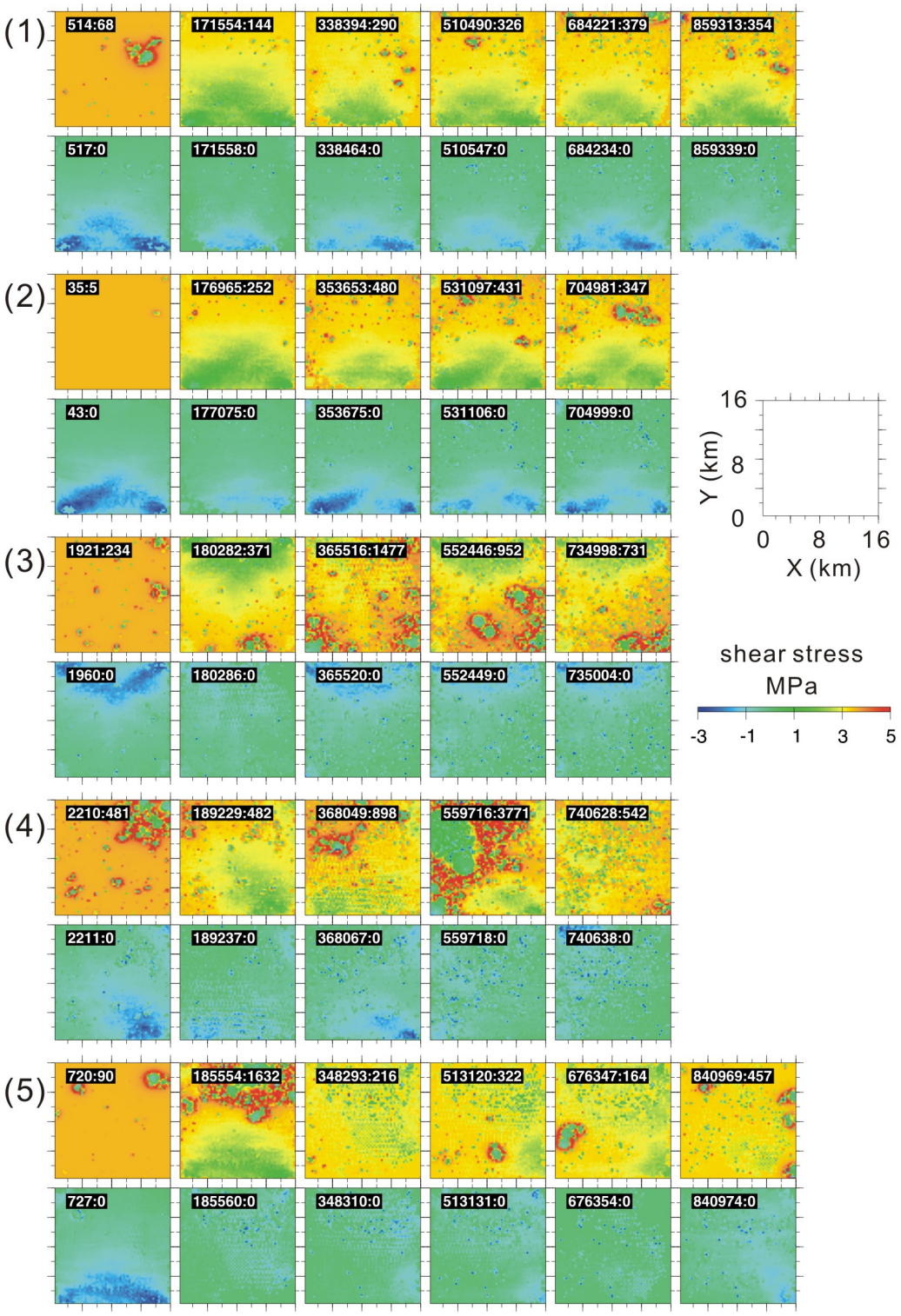

Figure 8: Stress field on the whole fault area before (upper row) and after (lower row) the characteristic earthquakes of each simulation (1) to (5). It should be made clear that the upper row corresponds to the earthquake preceding the characteristic event. The numbers separated by a colon represent, respectively, the event time in hours and the sequence number in each cycle (0 for the characteristic one). Each panel shows the entire fault regions of 16.4 km x 16.4 km.

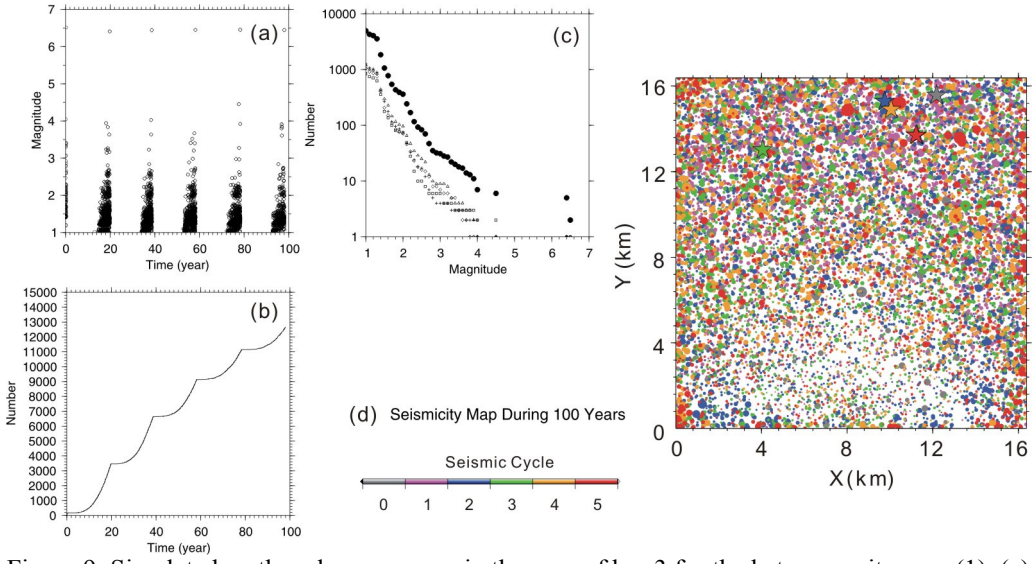

Figure 9: Simulated earthquake sequences in the case of k = 3 for the heterogeneity map (1). (a) Magnitude-Time, (b) Earthquake cumulative number – Time, (c) Size distribution and (d) Hypocenter distribution. See also the captions of the previous figures.

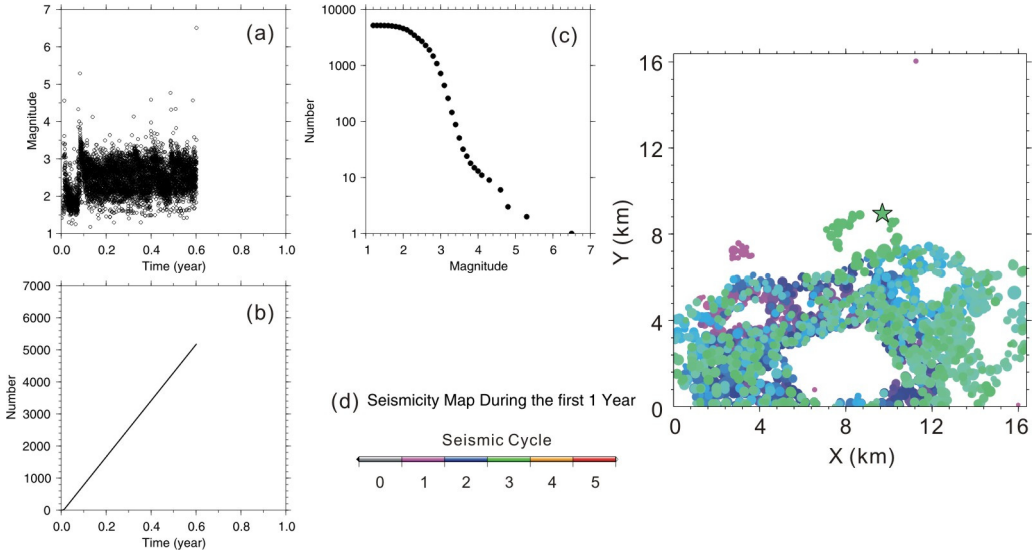

Figure 10: Simulated earthquake sequences for k = 60 on the heterogeneity map (1). Cumulative earthquake number against magnitude on the left panel and stress evolution for every 200 events in right panel.